A LOW ENERGY SENSOR FOR AUV-BASED JELLYFISH TRACKING

Jason Rife and Stephen M. Rock
Stanford University, CA 94305
and Monterey Bay Aquarium Research Institute, Moss Landing, CA 95039
Phone: 650-723-3608. Email: jrife@arl.stanford.edu, rock@arl.stanford.edu

ABSTRACT

This work describes optimization of a field-tested jelly tracking system to enable AUV deployment under tight energy constraints. Inspired by research in marine biology, the task of long duration jellyfish tracking poses both an opportunity and a significant challenge for the AUV community. AUVs offer the potential for extended midwater deployments, enabling observation of natural phenomena during periods of 24 hours or more. To establish task feasibility, a prototype visual tracking system was tested in the ocean aboard MBARI ROV Ventana. *These experiments successfully tracked a target jelly for ten minutes while consuming energy at a rate of 4 kW. AUV deployment will require dramatic reductions in power consumption, down to a level of approximately 10 W. An analysis of transmission and scattering losses leads to physical scaling expressions that describe sensor power consumption. Optimization of these scaling expressions suggests methods for achieving the significant power reduction necessary to transfer the ROV-based jelly tracking system to an AUV platform.*

1. INTRODUCTION

In the next decade, marine biologists will harness autonomous underwater vehicles (AUVs) to collect massive quantities of data *in situ*. First generation marine biology AUVs will undertake tasks currently performed by remotely operated vehicles (ROVs). Repetitive tasks, notably transecting, are highly conducive to automation. During a single day of research, a fleet of autonomous vehicles will sweep a far larger volume of water than a single tethered ROV. This capability for multiple simultaneous deployments will vastly increase the amount of data available to scientists. Autonomous operations will also free valuable ship time, allowing scientists to focus their limited resources on non-repetitive research tasks.

A second generation of AUVs will push beyond the capabilities offered by ROVs, allowing marine biologists to propose studies impractical given current technology. Unmanned and untethered, AUVs are well suited to data collection over durations of many hours, or perhaps days. Marine biologists routinely ask questions difficult to study without an extended presence in the midwater. This match between biologist vision and AUV capability promises to uncover a wealth of information concerning ocean ecology.

Jelly tracking represents a specific task that will leverage the AUV capability for long duration deployment. A jelly tracking AUV will first deploy to depths between 100-600 m, with possibilities for later deployments at greater depths. Missions will last for 24 hours or longer, depending on the nature of the research. Jelly tracking requires a sensor to measure relative position between vehicle and gelatinous target. This sensor must function flexibly for gelatinous animals of varying size and species, collectively designated in this work by the term “jellies.” Sample targets include 3-cm wide hydromedusae, 20-m long siphonophores, and 10-cm wide larvaceans.

Figure 1. Artist’s concept of an AUV tracking a target jellyfish.

Jellies make ideal targets for an extended duration AUV mission, as these fragile animals are slow moving with limited ability to sense their surroundings. These gelatinous marine animals are delicate, often too fragile to survive transport and study under laboratory conditions. A jelly tracking vehicle could observe a target over a long duration, providing accurate *in situ* information without disturbing or damaging the specimen. By producing a time-lapse video sequence, the AUV will answer a range of questions concerning jelly behavior and ecology. CTD and inertial sensors will provide valuable supplemental data for some research tasks. In principle, the jelly tracking sensor might provide information about non-gelatinous denizens of the midwaters, as well.

This work examines methods for transferring an ROV-based jelly tracking sensor to an AUV platform. Section 2 describes successful field trials of a jelly tracking sensor using MBARI ROV *Ventana*. Subsequent sections outline methods for achieving power reductions required for an AUV platform. Specifically, section 4 explores alternate low energy sensing technologies. Section 5 discusses optimization of the baseline visual jelly detector.

2. FROM ROV TO AUV

2.1. Ocean Experiment Hardware

Implementation of a prototype jelly tracking system proves concept feasibility and establishes the nature of hurdles stemming from operation in the open ocean. The ROV-based jelly tracker proves useful in its own right, as a pilot-assist tool. The tracker automates stressful, repetitive tasks ordinarily performed by a human operator, allowing the ROV pilot to focus on higher level concerns.

The prototype sensor relies on optical jelly detection. Images were captured using a Sony HDC-750A camera operating at 100-600 m depth. The camera was mounted on MBARI ROV *Ventana*, one of the two principle ROVs operated for marine biology research in the Monterey Bay [1]. Video signals travel via a 2000 m fiber between the submerged robot and the surface support vessel, R/V *Point Lobos*. On board the support vessel, a 700 MHz Pentium III vision computer receives the video signal. Figure 3 depicts jellies in two sample frames snapped in the Monterey Bay. The vision-processing algorithm segments candidate jelly targets from the video sequence and identifies the most likely candidate as the target. Recognition routines distinguish the target from other animals and detect possible out-of-frame events. Bearing is estimated at the centroid of the target region. A PD controller holds the target on the optical axis of the ROV camera. Control commands are routed through a pilot joystick and subject to a manual override, to ensure safe operation of the submersible. These signals travel along the umbilical to the ROV thrusters. The umbilical also carries power to the ROV from the support ship. The total power budget allots 8 kW among lighting (3.4 kW), systems (1.1 kW), and science (3.5 kW). Further details concerning the prototype visual tracking system are discussed in a separate reference [11].

2.2 Experimental Results

The prototype vision system was tested with a series of experiments in Monterey Bay during summer, 2000. The jelly tracking system closed the loop on two degrees of freedom: yaw and vertical translation. The prototype system included no mechanism for range estimation. A human pilot corrected range to keep the vehicle from drifting fore or aft. The ROV first tracked a specimen of genus *Mitrocoma*, for a one minute duration. A second experiment tracked *Phacellophora camtschatica* for two consecutive ten minute periods, interrupted by the appearance of a large group of squid. Fully automated tracking, with no pilot intervention, will occur during experiments in the second half of 2001.

Figure 2. MBARI ROV *Ventana*.

The successful implementation of an ROV based pilot-aid supports the notion of a fully automated jelly tracking system for AUV applications. Two major challenges complicate transfer of the pilot-aid technology to an untethered platform. First, AUV missions demand an increase in system reliability to achieve tracking times longer than the 10 minutes demonstrated during Monterey Bay experiments. Increased reliability requires better pattern recognition, a challenge given low target-to-background contrast, deformation of the jelly during swimming, and rotations of the target outside the image plane. Second, AUV applications demand dramatically

reduced power consumption. This work will concentrate on the second challenge, that of reducing power to a level suitable for AUV deployment.

2.3. ROV and AUV Power Requirements

Comparison of energy budgets for AUV and ROV establish the relative power reduction required to transfer the jelly tracking prototype to an autonomous platform. A cursory survey of sensors designed for other AUV applications frames the power estimate. Energy storage considerations further aid in fixing the power budget. Together these concerns result in a power budget of approximately 10 W, as developed in subsequent paragraphs.

To date, researchers have tested a range of sensors as low-energy payloads for autonomous vehicles. Of the sensors designed to interrogate the surrounding water using chemical, acoustic or visual signals, energy usage is typically in the 5-100 Watt range. As examples of general purpose AUV sensors, Langebrake et al. report testing of a chemical sensor (6W), a shadowed particle profiler (70 W), and a laser line scan bottom profiler (60 W) [6]. Short et al. detail a mass spectrometer that consumes less than 100 W [13].

For a sensor drawing power at a given rate, AUV endurance depends on its energy source. In current applications, AUVs typically use nickel-cadmium batteries, which offer energy density of approximately 55 Wh/kg. In the next decade, fuel cells may become readily available, if somewhat expensive. Proton exchange membrane fuel cells are expected to provide energy densities in the 200-1000 Wh/kg range [8].

Figure 3. Detection of jellies under direct illumination. Top: *Solmissus*. Bottom: *Colobonema*.

It is useful to relate energy budgets for two hypothetical missions, the first a 5-hour transect, the second a 24-hour jelly tracking task. For the long duration jelly tracking task, as compared to the shorter transecting task, energy efficiency takes on enormous importance. Fortunately, gelatinous animals move slowly relative to the surrounding ocean. These animals frequently remain stationary for minutes at a time. An autonomous vehicle following one of these animals will expend far less power in translation and bearing correction than an AUV performing a transect. The reduced consumption rate permits the same battery payload to actuate the AUV over a significantly longer duration. A large approximation, but a useful one, assumes that battery payload for propulsion will be roughly equivalent for a 5-hour transecting mission and a 24-hour jelly tracking mission. Though only a rough estimate, this statement reflects the fact that actuation power requirements do not seem unreasonable for the jelly tracking task. Rather, the onus of energy conservation lies with the sensor.

To calculate a rough estimate of maximum power draw for an AUV jelly sensor, it is convenient to persist the comparison of transecting and jelly tracking missions. With the assumption of similar overall energy storage capacity and similar propulsion requirements over the span of the mission, energy available for the sensing task is comparable for the two missions. A 5-hour transect involving the 60 W laser line scanner demands a bank of 5.45 kg of NiCad batteries dedicated to sensing. For a 24-hour jelly tracking mission, the same 5.45 kg NiCad battery payload permits a jelly sensor that draws no more than 12.5 W. After rounding down to denote the approximate nature of this figure, the allowable energy budget for jelly sensing is 10 W.

By comparison, sensor power requirements during ROV ocean trials were approximately 4 kW. Lighting alone accounted for a whopping 3.4 kW, with additional costs for camera operation and image processing. Clearly, power consumption issues require close examination before recommending the prototype ROV-based jelly tracker as a practical AUV payload. The following sections consider methods for improving energy requirements for a jelly sensor, first by using alternative sensing technologies, and second by optimizing visual sensing.

3. ALTERNATIVE SENSOR TECHNOLOGIES

3.1 Sensor Constraints

A visual sensor offers advantages as a jelly tracking technology. Visual sensors produce high signal to noise ratio when detecting actively illuminated jellies. Images

create a rich description of the natural environment, permitting machine vision applications including pattern recognition for target discrimination and reacquisition. Also, visual sensors and luminaires are commonly used for underwater applications, so custom hardware need not be developed. Despite these strong positives, an alternative sensor technology might be attractive for its power consumption benefits.

Any alternative sensor must meet the non-contact constraint. The inherent fragility of gelatinous species, coupled with the nature of the science mission, leads to this requirement. Although a beacon attached to the jelly would greatly simplify the tracking task, researchers lack a method of tagging animals without tearing or damaging gelatinous tissue. Sensors that require contact with the target are also likely to disturb jelly behavior or physiology. In order to obtain useful biological data, the jelly tracking vehicle should maintain a fixed standoff distance from the target.

3.2. Jelly Tracking in Nature

A search for alternative sensing technologies should commence with the natural world, which has already evolved a range of highly efficient jelly tracking sensors. In the upper ocean, many predators rely on scattering of sunlight to reveal their gelatinous prey. Reflections from jelly internal organs, refraction at the jelly-ocean interface, and scattering from internal colloidal suspensions all contribute to the discovery of jellies by visual predators, despite the natural camouflage of transparency.

Sighting distances may be increased, in some cases, by searching outside the visible spectrum. Recent work suggests some predators use ultraviolet radiation to their advantage. Gelatinous animals living in the upper ocean need to protect their tissue from the deleterious effects of ultraviolet light. UV-protective pigments absorb these rays, preserving jelly tissue, but at the risk of leaving an ultraviolet shadow visible to predators swimming below [5].

Evidence suggests that other predators employ polarization vision to increase detection range. Gelatinous tissues reduce partial polarization of transmitted light relative to strong linear polarization in ambient illumination. Shashar studied squid predation in the presence of neutral and polarization-active beads, the latter meant to represent jellies. Squid initiated attacks on the polarization-active beads from ranges 75% greater than their attacks on neutral beads [12].

As a technology for jelly tracking, natural light (passive) vision offers an enormous power advantage. On the down side, passive vision suffers from limited ambient lighting at night and in the depths. Nonetheless, passive optical detection of jellies, perhaps enhanced by ultraviolet or polarization sensitivity, could permit low-power initial acquisition of a jelly target. Some jelly species travel into food-rich surface waters for brief periods of time. Passive vision could be used to detect those species in surface waters, with a switch to active vision at greater depths.

3.3. Acoustics

Sonar offers potential for low-energy jelly detection. Unfortunately the close matching of acoustic impedance between jellies and surrounding ocean water results in very low signal strength for acoustic waves reflected from jelly targets. *In situ* measurements indicate extremely weak target strengths for common jelly species [9,14]. Although it is possible to vary the wavelength of a sonar system, acoustic wavelength must be chosen smaller than the jelly diameter. Past studies of acoustic target strength for common jellies have used wavelengths near 1 cm (120-420 kHz). Other regions of the acoustic spectrum are not expected to produce a stronger return signal.

One of the principle advantages of sound over vision is low absorption over long distances. Because the jelly tracking task employs sensing over short distances, of order 1 m, and because of weak signal reflection, it is not clear that active acoustic detection offers any strong advantage over active optical detection. Further study will be required to determine if receiver power consumption, resolution, or penetration of turbid waters gives the active sonar any edge over vision.

Passive sonar detection, despite extremely low energy requirements, offers little utility for the jelly tracking task. Gelatinous animals do not act as significant sound sources, and so may not be directly identified by a passive listener. Nor would one expect acoustic daylight, the background noise produced by ship traffic and wave action, to reveal the presence of a jelly target. Acoustic daylight studies have identified only large, solid shapes [2]. Moreover, background ocean noise, substantial at longer wavelengths, becomes very small (approximately 20 dB/μPa) for the 1 cm wavelengths useful to the jelly tracking application.

4. OPTIMIZING THE VISUAL SENSOR

4.1. Wave Transmission in the Ocean

This section discusses methods for optimizing the illumination environment for an active visual sensor. It is not clear that alternative sensors offer strong advantages over visual sensors for jelly tracking. For this reason, we investigate methods for optimizing the baseline visual system tested aboard the *Ventana* ROV. Because of similarities between the mathematical description of visual and acoustic wave propagation, these optimization results remain relevant for sonar applications.

In active sensing, the energy source emits radiation that scatters or reflects from the target back to a receiver. Power requirements for the source, which are geometry

dependent, sum with fixed receiver requirements to form the total energy budget. Variations in geometry influence transmission losses for waves traveling from source to receiver. Analysis of these transmission losses requires ray propagation techniques. The following irradiance equation, Equation 1, and diagram, Figure 4, describe propagation losses along the path between source and receiver:

$$I_s = I_r \cdot \left[\eta T(\alpha, \mathbf{p}) \frac{D_s^2}{D_m^2} \frac{D_j^2}{4R_r^2} \exp\left(-c(\lambda) \cdot (R_s + R_r)\right) \right]^{-1} \qquad (1)$$

I_s	Irradiance at source
I_r	Irradiance at receiver
D_s	Diameter of source
D_m	Diameter of measurement volume
D_j	Diameter of the smallest sphere enclosing jelly
R_s	Distance from source to jelly
R_r	Distance from jelly to receiver
T	Target scattering/reflection function
α	Angle between source and receiver axes
β	Angle from source center to receiver center
p	Jelly orientation vector
c	Coefficient of attenuation by medium
η	Source energy conversion efficiency
λ	Wavelength of light

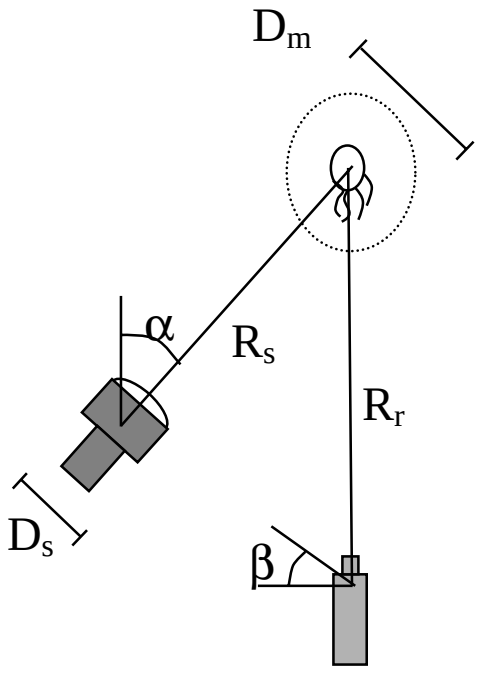

Figure 4. Source and receiver geometry for active sensing.

Two terms of Equation 1 model system hardware. The conversion efficiency term, η, accounts for an imperfect source, with efficiency defined as the wave energy output for a given battery power input. I_r indicates receiver resolution, defined as the minimum energy signal detectable by the receiver. All other terms account for transmission losses as waves travel from source to target and from target to receiver.

Inverse-square spreading losses dominate irradiance attenuation as waves travel from source to target. In three dimensions, light and sound waves propagate without dispersion, such that the response to an impulse disturbance creates a hollow shell expanding at the wave speed. As the spherical shell travels away from the point disturbance, its area grows as radius squared. Energy conservation over the surface results in the famous inverse-square law: irradiance (energy per unit area) varies inversely with radius squared. Directional sources are more useful than isotropic point sources for the jelly tracking task. Directional sources also suffer from inverse-square spreading losses, although, in many cases, the center of spherical spreading stands significantly behind the physical location of the source device. For jelly tracking, it is most convenient to calculate inverse-square scaling using diameter of the source cone, a quantity easily measured in practice. From jelly to target, spreading losses result in an attenuation of D_s^2/D_m^2.

Gelatinous tissue redirects only a small fraction of impinging wave energy, the remainder of which transmits through the target jelly's body. Equation 1 includes a dimensionless target transfer function, $T(\alpha,\mathbf{p})$, to account for the directional dependence of this small fraction of redirected energy. The transfer function represents the ratio of outgoing to incoming fluxes, where the incoming and outgoing directions are separated by an angle, α, for a jelly with a particular orientation, **p**. The transfer function is made dimensionless by defining it on a sphere of radius D_j, the minimal sphere diameter enclosing the jelly. The definition is equivalent to common dimensional expressions of reflection and scattering functions, defined with units of sr^{-1}. The transfer function lumps together a set of physical phenomena difficult to evaluate independently: absorption, scattering, and reflection. The complexity of these phenomena implies that experiments are required to evaluate $T(\alpha,\mathbf{p})$. For the purpose of this work, it is sufficient to note that $T(\alpha,\mathbf{p})$ is a small number.

Waves exiting the jelly undergo further spreading losses during transmission from target to receiver. In Equation 1, the $D_j^2 / 4R_r^2$ term expresses the spreading loss as a nondimensional ratio of spherical areas. Absorption by the medium further attenuates propagating waves. Absorption losses increase exponentially with propagation distance. In Equation 1, the attenuation coefficient, c, and the travel distance, R, have units of inverse length and length, respectively. For acoustic waves traveling short distances, absorption loss is negligible. For light waves, the attenuation coefficient

varies spectrally, becoming quite large for wavelengths above and below 480 nm, as measured in air. The optical attenuation coefficient, c, combines absorption and scattering by the medium. Absorption converts light energy into heat, while scattering from particles suspended in the water column merely redirects the light path. Because particle concentration varies, the attenuation coefficient depends on ocean conditions at a given time and location. For typical ocean conditions, attenuation of blue light traveling 1 meter to and from a target results in 10% energy loss [7].

4.2. Optimizing Lighting Configuration

Task specific illumination promises significant reduction in sensor power consumption. The prototype jelly tracking system operates in two distinct modes, with distinct lighting requirements. The jelly tracker must first locate its target. This initialization procedure requires broad ROV-style lighting for a brief period of time. After initialization, the jelly tracker enters a regulation mode. For this mode, in which the jelly tracker spends most of its time, the jelly remains at a fixed position relative to the vehicle, subject to slight disturbances. Spot lighting is sufficient for this regulation task.

Introducing Equation 2 as a cost function permits power optimization through variation of spot light geometry:

$$P_s = I_s D_s^2 = \frac{1}{\eta} I_r \cdot \frac{D_m^2}{D_j^2} e^{c(\lambda)R_s} \cdot \frac{1}{T(\alpha, \mathbf{p})} \cdot 4R_r^2 e^{c(\lambda)R_r} \qquad (2)$$

Equation 2 expresses source power requirements (Watts), rather than irradiance requirements (Watts/m^2), but otherwise equals Equation 1, after multiplication by D_s^2. The terms of Equation 2 are separable. Since each term depends on distinct parameters, the terms may be independently minimized. The resulting optimization problem is trivial, with the interest lying in the design constraints that govern energy minimization.

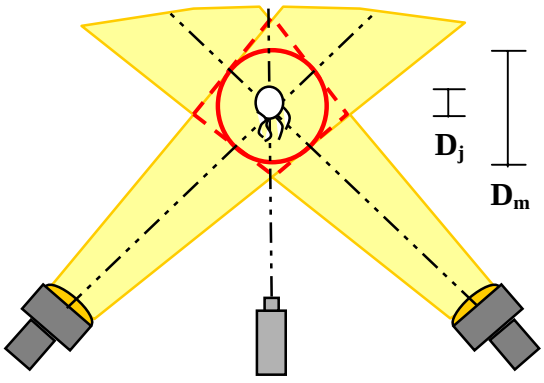

Figure 5. The Measurement Volume can be visualized as the included sphere defined by the intersection of multiple illuminating cones.

Definition of Measurement Volume and Margin Ratio: Measurement volume diameter, D_m proves critical in minimization of spreading losses from source to target. Formally, D_m is defined as the diameter of the circular intersection between the illumination cone and the plane, normal the cone axis, which passes through the target jelly's centroid. This diameter helps establish a three-dimensional tracking envelope around the target jelly. The tracking vehicle will detect the target jelly as long as the vehicle steers to maintain its target within the spherical volume defined by D_m.

The concept of a measurement volume makes particular sense in the context of multiple light sources. Using multiple light sources, rather than a single one, provides better uniformity across the measurement volume and less sensitivity to target orientation. When multiple light sources are designed to converge near a nominal target location (R_c), they define a kite shaped region within which the target will shine brightly. For moderate lighting angles (α between 20-70°) and small beam spreading angles, a sphere, of diameter D_m, describes the kite-shaped measurement volume sufficiently well for scaling purposes.

The jelly tracking task places less emphasis on the exact diameter of the measurement volume than on its size relative to the target jelly. To this end, the margin ratio, M, is introduced to describe the relative sizes of the measurement volume and the target jelly:

$$M = \frac{D_m}{D_j} \qquad (3)$$

Minimizing Source-to-Target Losses: Optimization of spreading efficiency requires minimization of D_m, or equivalently of M. Power consumption, P_s, varies quadratically with M, and would reach a trivial minimum in the absence of constraints. For sensors detecting a contrast between background and jelly, this constraint demands M exceed unity. At unity M, a centered jelly occupies the entire field of view and segmentation strategies separating the target from the background become ineffective. For sensors employing texture-matching routines (i.e., correlation), the minimum M constraint depends on sensor resolution, sampling time, target texture, and the time scale of vehicle dynamics.

Source diameter, D_s, does not factor into the optimization. A change in source diameter necessitates a change in source irradiance in order to preserve a given level of I_r, all else equal. Likewise, beam spreading angle and the source-to-target range, R_s, do not influence inverse-square spreading losses. These factors trade, so that at larger ranges, a smaller spreading angle results in a constant value of D_m. R_s enters the optimization

through the absorption term only. Because absorption has little effect on blue wavelengths over short distances, the optimization displays weak sensitivity to the absorption term. For practical purposes, the optimization can be considered independent of R_s when using illumination near the blue.

Absorption cannot be neglected for all wavelengths, however. Spectral variation in the attenuation term results in maximum penetration for blue-green lighting (near 480 nm). At longer wavelengths, attenuation increases rapidly as shown in Table 1.

Evolution has not ignored the fact that blue light penetrates water more effectively than other wavelengths. Underwater animals display more sensitivity to the blue wavelength than to other parts of the electromagnetic spectrum. Because many jellyfish possess light sensing statocysts, it is important to consider illumination wavelength in designing the jelly tracking system. An efficient design illuminates at a wavelength as close as possible to 480 nm without substantially interfering with jelly behavior. As no data is available to analyze this trade-off between lighting penetration and minimal behavioral impact, the issue remains open. Note that illumination in the ultraviolet is not acceptable, because UV light causes damage to gelatinous tissue [5].

Color	λ	Attenuation over travel distance of 2m
Blue	480	10%
Orange	580	33%
Near Infrared	820	98%

Table 1: Spectral absorption of light over a 2 m travel distance

Minimizing Target-to-Receiver Spreading Losses:
In the absence of absorption, energy costs rise quadratically with target-to-receiver distance, R_r. Absorption only augments this quadratic dependence. Any reduction in standoff distance between the receiver and the jelly produces a very strong improvement in the sensor energy budget.

Scientific requirements constrain this minimization, placing a lower bound on R_r to prevent intrusion by the AUV into the target jelly's habitat. It is convenient to introduce an expression for this minimum distance, the biological standoff distance, B. Because the jelly can be expected to travel anywhere in the envelope defined by the measurement volume, the minimum nominal camera to jelly distance, R_r, should equal the biological standoff distance plus the measurement volume radius:

$$R_r = D_j(B + \tfrac{1}{2}M) \qquad (4)$$

With target dimensions varying widely, it is important to express B nondimensionally. In Equation 4, the biological standoff distance, B, has been expressed as a multiple of the jelly diameter, D_j.

In field experiments, the dominant vehicle-jelly interactions were hydrodynamic, resulting from thruster wash or vehicle wake. It may be possible to reduce these interactions by placing the camera on a narrow sting projecting from the vehicle. This strategy would greatly improve the power budget by effectively reducing the required biological standoff distance, B.

Minimizing Target Scattering Losses:
The target transfer function, $T(\alpha, \mathbf{p})$, governs recovery efficiency of the signal returned by the target jelly. Because the tracking vehicle has no control over jelly orientation, expressed as the vector $\mathbf{p}$, design optimization considers only the source-to-receiver angle, α. The sensitivity of the transfer function to α remains unknown. Although researchers have investigated scattering in jellyfish at a subcellular level, no bulk scattering data is currently available. [4]. If the target transfer function were determined experimentally, energy optimization would require simply that the light source be positioned to maximize $T(\alpha, \mathbf{p})$.

In practice, α strongly affects signal to noise ratio, a relationship not indicated by Equation 2. Specifically, lighting angle affects ambient illumination through backscatter from particles suspended in the water column. The resulting veil of background light sets a noise threshold for target detection. For a given target, the noise threshold implies a maximum detection range, beyond which inverse-square spreading attenuates target illumination below backscatter fluctuation noise.

The magnitude of scattering depends on two factors, first, the relative angle between light rays impinging on and leaving from the scattering particles, and second, the

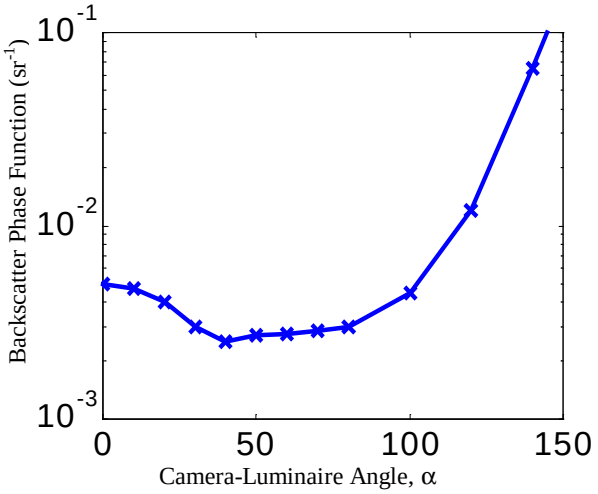

Figure 6. Experimental data for phase function (exiting radiance normalized by impinging irradiance, units sr^{-1}) for volumetric scattering by ocean water illuminated at 530 nm. Plot adapted from the M phase function reported by Gordon [3].

lighted depth along a line through the receiver. Given narrow spot illumination and narrow camera field of view, only primary scattering need be considered. A narrow camera field of view implies that scattered light enters only from the direction of the measurement volume, centered around backscatter angle α. Figure 6 depicts scattering intensity as a function of α, measured volumetrically in ocean experiments using illumination at 530 nm. The plot, adapted from Gordon, shows that backscatter is relatively flat for α between 40 to 80° [3].

Lighted depth also affects backscatter intensity. Lighted depth is effectively the axis of the measurement volume kite parallel the camera optical axis, as depicted in Figure 5. For α near zero, the kite approaches infinite depth, with penetration distance bounded only by optical absorption in the medium. For α near 90°, lighted depth approaches D_m.

Combining lighted depth and phase function effects, minimum backscatter is expected for α in the 30-40° range. Unless the transfer function T varies strongly with α, these background scattering concerns will dictate the choice of α.

4.3. Optimizing Duty Cycle

Whereas the previous section considered variations in spatial variables, this section considers variations in temporal variables to achieve power reduction. Specifically, the section focuses on strobed lighting characterized by a pulse duration and a period between pulses. The ratio of pulse duration to period is commonly referred to as duty cycle. For visual sensors, pulse duration is determined by receiver exposure requirements. Duty cycle may be varied by matching illumination time to receiver integration time and by reducing the interval between flashes. In principle, strobed lighting can significantly reduce power requirements averaged over time.

This discussion assumes a source that permits rapid switching. Such light sources, light emitting diodes, for instance, can cycle from no power to full power in microseconds. Many underwater lighting sources do not permit rapid switching, and hence, do not permit variation in sample period. Efficient underwater light sources, like the arc lamps and high intensity discharge luminaires commonly mounted on ROVs, require significant start up times. Arc lamp restart times fall in the 5-10 second range. Lamp drivers, available for some ROV lighting systems, do allow rapid transitions between full and partial loading. These drivers cannot shut off completely, with minimum loading commonly at 10% maximum power [10].

With a rapid-switching source assumed, the major liability of sensing with a long sample period is loss of the jelly target from the measurement volume. For this reason, duty cycle cannot be discussed independently of the margin ratio, M. To be useful an energy scaling expression should fix the risk of the target wandering outside the measurement volume. As sample period drops, margin ratio must increase to preserve the probability of recovering the target jelly in a successive image.

The energy ratio, E, expresses the ratio of average power consumed by two lighting systems, denoted A and B. Duty cycle multiplies pulse power to obtain a time averaged expression, with τ_d equal pulse duration and τ_p equal pulse period.

$$E = \frac{\left(\tau_{d,A} / \tau_{p,A}\right) P_{s,A}}{\left(\tau_{d,B} / \tau_{p,B}\right) P_{s,B}} \qquad (5)$$

Here, the expression for power leaving the source, P_s, may be expanded using Equation 2. Several terms from the expansion cancel given reasonable assumptions. If both systems observe the same target, the ratio of scattering functions, $T(\alpha,\mathbf{p})$, vanishes. Fixing source efficiency, receiver resolution, and receiver exposure requirements removes dependence on η, I_r, and τ_d. Lastly, if we assume illumination near 480 nm, we may neglect the absorption exponential term as small. The remaining terms give the following expression:

$$E = \frac{\tau_{p,B}\ M_A\ R_{c,A}^2}{\tau_{p,A}\ M_B\ R_{c,B}^2} \qquad (6)$$

Further simplification of the expression requires a relation among the parameters τ_p, M, and R_c. Equation 4 has already established an optimal relation between R_c and M. To express sample period, τ_p, in terms of the margin ratio, M, assume that the measurement volume diameter, D_m, is sufficiently large that the jelly cannot escape from inside the measurement volume. A simple kinematic scaling states that if the jelly is capable of an acceleration, a, and if the jelly begins at the measurement volume center with zero velocity relative to the tracking vehicle, that the relative displacement after a period τ will be no more than:

$$\tfrac{1}{2} D_m = \tfrac{1}{2} a \tau_p^2 \qquad (7)$$

The maximum relative displacement should fall within the radius of the measurement volume, expressed here in terms of D_m. Equation 7 assumes no small-scale ocean turbulence or velocity gradient. In the absence of a tether, other disturbance loads on the AUV are assumed small. Rewriting Equation 7 in terms of M gives

$$M = \frac{a}{D_j} \tau_p^2 \qquad (8)$$

Combining Equations 4-8, the following expression results for the ratio of energy usage by system A as compared to usage by system B.

$$E = \frac{\tau_{p,A}}{\tau_{p,B}} \left(\frac{B + \frac{a}{2D_j} \tau_{p,A}^2}{B + \frac{a}{2D_j} \tau_{p,B}^2} \right)^2 = \left(\frac{M_A}{M_B} \right)^{\frac{1}{2}} \left(\frac{2B + M_A}{2B + M_B} \right)^2 \quad (9)$$

In final analysis, Equation 9 supports the result that longer sample periods degrade the overall energy budget. The margin ratio, *M*, should be minimized, and sample period, τ_p, should be set accordingly.

Applying this rule allows prediction of a suitable sample interval for jelly tracking. Section 4.2 establishes that *M* must be at least unity for a sensor identifying the jelly by contrast with the background. For this analysis, take *M* to be unity. Observations of jellies in the open ocean suggest that small jellies, of approximately 5 cm in diameter, can move no more than one body length in a second. These statements, together with Equation 8, imply that a jelly tracker might conceptually function at a fixed sample rate of approximately 1 Hz. For typical camera exposure times, on the order of 10 ms, the resultant duty cycle improves the overall energy budget by a factor of 100 as compared with continuous illumination.

5. CONCLUSION

Requirements are discussed for a jelly tracking AUV, a vehicle intended to support midwater research by marine biologists. AUVs offer an advantage over ROVs in that they open the possibility for extended duration missions. To promote a 24-hour deployment, the jelly tracking sensor should operate using approximately 10 W power. A prototype visual tracking system was tested in the ocean aboard ROV *Ventana*. The system successfully tracked a target jelly for ten uninterrupted minutes, using 4 kW for sensing. Dramatic reductions in the energy budget for illumination would be required to transfer the prototype to an AUV platform. To this end, ray propagation techniques were applied to the jelly tracking task to generate recommendations for decreasing power consumption:

- Reduce margin ratio, *M*, to the minimum level possible (i.e., $M \approx 1$ for a contrast detector)
- Reduce R_c to the minimum level permitted for biological experiments, according to Equation 4
- Place imaging sensor on a sting to reduce *B*
- Illuminate at a wavelength slightly above 480 nm, to minimally affect jelly behavior while maximizing light penetration
- Match sample period to jelly acceleration, according to Equation 8

Application of these rules will likely result in a jelly sensor that operates at the desired 10 W level.

We thank MBARI and Packard Foundation grants 98-3816 and 98-6228 for supporting this work.

6. REFERENCES

[1] R. Barber. "Deep Ocean Research Using Computer Controlled ROVs", *Sea Technology*, 30, pp. 47-49, 1989.

[2] M. Buckingham, J. Potter, C. Epifanio. "Seeing Underwater with Background Noise," *Scientific American (International Edition)*, v. 274, no. 2, p. 40-44, Feb. 1996.

[3] H. Gordon. "Modeling and Simulating Radiative Transfer in the Ocean," *Ocean Optics*, ed. R. Spinrad, K. Carder, M. Perry, Oxford University Press, p. 3-39, 1994.

[4] S. Johnsen, E. Widder. "The Physical Basis of Transparency in Biological Tissue: Ultrastructure and the Minimization of Light Scattering," Theoretical Biology, v. 199, p. 181-198, 1999.

[5] S. Johnsen, E. Widder. "Ultraviolet Absorption in Transparent Zooplankton and its Implications for Depth Distribution and Visual Predation," *Marine Biology*, v. 138, p. 717-730, 2001.

[6] L. Langebrake, S. Samson, E. Kaltenbacher, E. Steimle, J. Patten, C. Lembke. "Sensor Development: Progress Towards Systems for AUVs/UUVs MTS Oceans 2000," *Proc. IEEE/MTS Oceans 2000*, 2000.

[7] L. Mertens. *In-Water Photography Theory and Practice*, Wiley-Interscience. p. 25. 1970.

[8] J. Mooney, *chair*, Committee on Undersea Vehicles and National Needs. *Undersea Vehicles and National Needs*, National Academy Press, p. 27, 1996.

[9] E. Mutlu. "Target Strength of the Common Jellyfish (Aurelia Aurita): a Preliminary Experimental Study with a Dual-Beam Acoustic System," *ICES Journal of Marine Science*, v. 53, p. 309-311, 1996.

[10] M. Olsson, D. Rimer, S. Parker. "ROV Lighting with Metal Halide," Deep Sea Power & Light White Papers, 2000.

[11] J. Rife, S. Rock. "Visual Tracking of Jellyfish *in Situ*," accepted for publication in *Proc. Intl. Conf. Image Processing*, 2001.

[12] N. Shashar, R. Hanlon, A. Petz. "Polarization Vision Helps Detect Transparent Prey," *Nature*, v. 393, p. 222-223, May 21, 1998.

[13] R. Short, D. Fries, M. Kerr, R. Byrne. "*In-Situ* Chemical Analysis Using Mass Spectrometry on Unmanned Underwater Vehicles," *Proc. IEEE/MTS Oceans 2000*, 2000.

[14] P. Wiebe, C. Greene, T. Stanton, K. Burczynski. "Sound Scattering by Live Zooplankton and Micronekton: Empirical Studies with a Dual-Beam Acoustical System," *Journal of the Acoustical Society of America*, v. 88, p. 2346-2360, 1990.